Indian Journal of Chemical Technology
Vol. 31, May 2024, pp. 346-354
DOI: 10.56042/ijct.v31i3.7503

# Transportation of SWCNT and MWCNT-based nanofluid through an exponentially stretching Riga plate in the presence of shear heating

Kiran Kunwar Chouhan & Santosh Chaudhary*

Department of Mathematics, Malaviya National Institute of Technology, Jaipur-302 017, India

*E-mail: kiranchouhanudr@gmail.com (KKC), d11.santosh@yahoo.com (SC)

*Received 22 December 2023; accepted 19 April 2024*

Nanofluids accomplish better results in heat transfer practices due to their exceptional thermal characteristics than traditional heat transfer fluids. This study reports the thermophysical behavior of carbon nanotube-based nanofluid flow through an exponentially stretched Riga plate, along with the contribution of variable dynamic viscosity, velocity slip, and viscous dissipation impacts. Nanofluid consists of single-walled carbon nanotubes (SWCNTs) and multi-walled carbon nanotubes (MWCNTs) in aqueous solution. Boundary layer flow is intended to be steady, laminar, viscous-incompressible, and two-dimensional. Governing system of partial differential equations is elucidated with pertinent similarity transformations into dimensionless form. Simplified mathematical model is numerically operated through the spectral relaxation method. Significance of sundry parameters over momentum and heat profiles are delineated via graphs. Also, inconsistencies in point-specific skin drag coefficient and Nusselt heat transfer index are conferred through acquired numerical data.

**Keywords:** Nanofluids, Riga plate, Slip effects, SWCNT and MWCNT-based nanofluid, Viscous dissipation

## Introduction

In recent times, advancement in the heat conductivity of conventional fluids is one of the prime interests in engineering, industry, and many technological processes. Choi and Eastman[1] proposed a potential method for improving fluid productivity known as nanofluids. Nanofluids are working fluids possessing improved thermal attributes, enabling broader applications in thermal processes. Several studies are conducted to perceive its relevance in various applications, including thermal energy storage, refrigeration system, electronics, biomedical, internal combustion engines, solar collectors, material processing, etc. Nanofluids are procured by suspension of nano-sized particles (e.g., carbon nanotubes, graphene, silica, gold, etc.) in the base fluids. Carbon nanotubes (CNTs) are tube-like polymorphic carbon structures with a high aspect ratio (length/diameter) and a diameter usually in the 1 to 100 nm range. Two types of CNTs have been used in the current study, single-walled carbon nanotubes (SWCNT) and multiple-walled carbon nanotubes (MWCNT). Kamali and Binesh[2] analyzed the heat transfer performance of MWCNTs based on non-Newtonian nanofluid flow in a straight tube, and the wall region dominates the heat transfer coefficient. Prabhavathi et al.[3] examined thermal characteristics of CNTs-based Maxwell nanofluid flow through a vertical cone. Chaudhary and Chouhan[4] depicted Joule and shear heating influence on copper-blood nanofluid flow subjected to a stretching surface. Recently, Eswaramoorthi et al.[5] considered CNT-glycerin nanofluid flow through a Riga plate with a Cattaneo-Christov heat flux model in a Darcy-Forchheimer porous medium.

The Lorentz force, impelled by the transverse magnetic and electric field and directed parallel to the surface, is effective towards the pressure-gradient-driven boundary layer. Gailitis and Lielausis[6] employed this concept of Lorentz force to influence the flow of an electrically conducting fluid through a Riga plate (Fig. 1). This plate comprehends an arrangement of permanent magnets with alternating magnetizing polarity and alternative electrodes arranged in a lined-up manner on a plane surface. This plate is advantageous in regulating the boundary layer flow and reducing skin friction and pressure drag by modulation of magnetic and electric field strength. Boundary layer flows over the Riga plate have recently gained much attention from researchers. Ayub et al.[7] considered buoyancy forces impact on nanofluid flow through the Riga plate with slip

boundary conditions and observed that fluid velocity is a decreasing function of nanoparticle flux and slip parameter. Nasir et al.[8] numerically investigated the velocity slip and thermal radiation effects on fluid flow towards an equilibrium point over an extending/contracting Riga plate. Recently, Shamshuddin et al.[9] theoretically scrutinized the thermo-solutal free convective flow through an exponentially stretching Riga plate.

Viscous dissipation is an irreversible phenomenon in which the kinetic energy of fluid transmutes into heat due to the action of shear forces on adjoining fluid layers. The impact of viscous dissipation was primarily examined by Brinkman[10]. A bunch of research studies concerning viscous dissipation impact in nanofluid flows is Ghalambaz et al.[11], Chaudhary and Kanika[12], and Mahesh et al.[13].

Velocity slip materializes when adhesion among fluid molecules gets more influential as against adhesion between fluid molecules and the solid surface at which fluid is flowing. Velocity and temperature slip effect occurs in many physical circumstances like emulsion and polymer solvents. This phenomenon has several uses in friction diminution in micro-channels, energy preservation, and polishing synthetic cardiac valves. Many researchers, Sinha et al.[14], Chaudhary and Choudhary[15], Gbadeyan et al.[16], and Krishna[17] undertook numerical and experimental studies concerning velocity and thermal slip effect on fluid flow in distinct circumstances.

Prior discussions have inspired the authors to embark on an exploration of nanofluid flow containing carbon nanotubes across a variety of surfaces and under diverse conditions. The current research focuses on comparing the characteristics of a nanofluid containing CNTs as it flows over a plate that is exponentially stretching, and where the viscosity of the nanofluid varies with temperature. This study represents novel research as it explores a topic that has not been previously investigated. The formulated mathematical model has been rendered in a non-dimensional format through meaningful similarity transformations. The system of ordinary differential equations (ODEs) derived from this model is then assessed using the SRM (Spectral Relaxation Method) technique, and the resulting graphical patterns of various parameters are examined and explained.

## Mathematical formulation

In the present investigation, two nanofluids' boundary layer flow is considered time-independent, two-dimensional, laminar, and viscous incompressible over an exponentially stretched Riga plate. Both nanofluids, SWCNT-water and MWCNT-water, are analyzed in a comparative manner. The impact of variable dynamic viscosity and viscous dissipation on the nanofluid flow is taken into consideration. The plate is stretched in the $x-$axis direction with a stretching velocity $u_s = u_0 e^{x/l}$, where $u_0$ is stretching constant and $l$ stands for characteristic length. The flow is propelled by a Lorentz force parallel to the surface, in a direction aligned with the ground. The $y-$axis takes on a vertical orientation relative to this force, and the $z-$axis measures the span-wise direction of the plate (Figs 1 & 2). The governing mathematical model is acknowledged as[18]

$$\frac{\partial u}{\partial x}+\frac{\partial v}{\partial y}=0 \qquad ...(1)$$

$$u\frac{\partial u}{\partial x}+v\frac{\partial u}{\partial y}=\frac{1}{\rho_{nf}}\frac{\partial}{\partial y}\left[\mu_{nf}(T)\frac{\partial u}{\partial y}\right]+\frac{\pi j_0 M_0}{8\rho_{nf}}e^{-\frac{\pi}{a_1}y} \qquad ...(2)$$

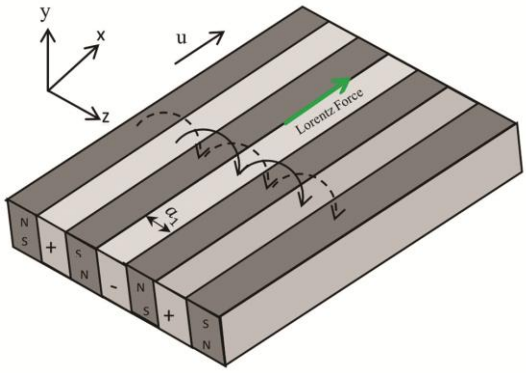


Fig. 1 — Diagrammatic setup of the Riga plate

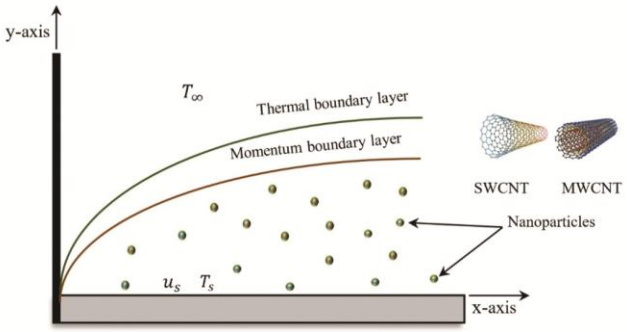


Fig. 2 — Diagrammatic configuration of the nanofluid flow

$$u\frac{\partial T}{\partial x}+v\frac{\partial T}{\partial y}=\frac{\kappa_{nf}}{(\rho C_p)_{nf}}\frac{\partial^2 T}{\partial y^2}+\frac{\mu_{nf}(T)}{(\rho C_P)_{nf}}\left(\frac{\partial u}{\partial y}\right)^2 \quad ...(3)$$

subjected to the boundary conditions

$$u=u_s+u_{slip},\ v=0,\ \kappa_f\frac{\partial T}{\partial y}=-h_s(T_s-T)\ \text{ at }\ y=0$$

$$u\to 0,\ \mathrm{T}\to \mathrm{T}_\infty\ \text{ as }\ \mathrm{y}\to\infty \quad \ldots(4)$$

whereat $u, v$ are nanofluid velocities in $x-$ and $y-$directions, respectively, subscript $nf$ stands for nanofluid, $\rho\left(=\frac{u}{\nu}\right)$ represents the density, $\mu$ refers the viscosity, $\nu$ is the kinematic viscosity, $T$ is the temperature of nanofluid, $j_0$ refers applied current density, $M_0$ represents intensity of applied magnetic effect, $a_1$ represents span of magnets and electrodes, $\kappa$ is heat conductivity, $C_p$ refers heat capacity constant pressure, $u_{slip}=d\frac{\partial u}{\partial y}$ is the slip velocity, $d$ is the slip velocity factor, subscript $f$ refers the base fluid, $h_s$ refers convective heat transfer coefficient, $T_s=T_\infty+T_0e^{x/2l}$ is the skin temperature, where $T_0$ is the reference temperature, and $T_\infty$ denotes ambient temperature. Table 1 presents thermo-physical values of nanoparticles and base fluid, and the physical models for nanofluid characteristics are stated as below[3]:

$$\mu_{nf}=\frac{1}{(1-\varphi)^{5/2}}\mu_f \quad \ldots(5)$$

$$\rho_{nf}=\left(1-\varphi+\varphi\frac{\rho_{CNT}}{\rho_f}\right)\rho_f \quad \ldots(6)$$

$$(\rho C_p)_{nf}=\left[1-\varphi+\varphi\frac{(\rho C_p)_{CNT}}{(\rho C_p)_f}\right](\rho C_p)_f \quad \ldots(7)$$

Table 1 — Estimates for thermal and physical values of carbon nanotubes and water[19]

| Sample | $\rho(kg/m^3)$ | $C_p(J/kgK)$ | $\kappa(W/mK)$ |
|---|---|---|---|
| *SWCNT* | 2600 | 425 | 6600 |
| *MWCNT* | 1600 | 796 | 3000 |
| Water | 997 | 4179 | 0.613 |

$$\kappa_{nf}=\frac{1-\varphi+2\varphi\frac{\kappa_{CNT}}{\kappa_{CNT}-\kappa_f}\ln\left(\frac{\kappa_{CNT}+\kappa_f}{2\kappa_f}\right)}{1-\varphi+2\varphi\frac{\kappa_f}{\kappa_{CNT}-\kappa_f}\ln\left(\frac{\kappa_f+\kappa_{CNT}}{2\kappa_f}\right)}\kappa_f \quad \ldots(8)$$

here, $\varphi$ refers to the volume concentration of nanoparticles in the fluid and subscript CNT stands for carbon nanotubes. The variable viscosity is considered as the inverse function of temperature, is given as follows[18]

$$\mu_{nf}(T)=\frac{\mu_{nf}}{\left[1-\delta(T_\infty-T)\right]} \quad \ldots(9)$$

where $\delta$ is a constant with dimension $\left\{T^{-1}\right\}$ and $\frac{\delta}{\mu_{nf}}$ is a constant which rely on thermal characteristic. Generally, $\frac{\delta}{\mu_{nf}}>0$ for liquids and $\frac{\delta}{\mu_{nf}}<0$ for gases.

Ensuing similarity transformation is engaged in the above-mentioned system of equations

$$\psi=\sqrt{2\nu_f u_0 l}e^{x/2l}f(\eta),\ \eta=\sqrt{\frac{u_0}{2\nu_f l}}e^{x/2l}y,\ \mathrm{T}=\mathrm{T}_\infty+T_0e^{x/2l}\theta(\eta) \quad \ldots(10)$$

where $\psi$ denotes the stream function, and the resultant system of ordinary differential equations is obtained as

$$\frac{f'''}{\left(1-\frac{\theta}{\theta_s}\right)}+\frac{f''\theta'}{\theta_s\left(1-\frac{\theta}{\theta_s}\right)^2}+\frac{\nu_f}{\nu_{nf}}(ff''-2f'^2)+\frac{\mu_f}{\mu_{nf}}Qe^{-\alpha\eta}=0 \quad \ldots(11)$$

$$\frac{\kappa_{nf}}{\kappa_f}\theta''+\mathrm{Pr}\frac{(\rho C_p)_{nf}}{(\rho C_p)_f}(f\theta'-f'\theta)+\frac{\mu_{nf}}{\mu_f}\frac{Br}{\left(1-\frac{\theta}{\theta_s}\right)}f''^2=0 \quad \ldots(12)$$

with boundary conditions

$$f(0)=0,\ f'(0)=1+\lambda_v f''(0),\ \theta'(0)=-\lambda_{\mathrm{T}}\left[1-\theta(0)\right]$$

$$f'(\infty)\to 0,\ \theta(\infty)\to 0 \quad \ldots(13)$$

In the above equations, $f$ and $\theta$ are dimensionless function of similarity variable $\eta$, prime ' expresses the differentiation with respect to $\eta$, $\theta_s = \frac{1}{\delta(T_\infty - T_s)}$ is variable viscosity parameter, $Q = \frac{\pi l j_0 M_0}{4\rho_f u_s^2}$ is modified Hartman number, $\alpha = \frac{\pi}{a_1}\sqrt{\frac{2l\nu_f}{u_s}}$ is dimensionless parameter, $\Pr = \frac{\mu_f (C_p)_f}{\kappa_f}$ is the Prandtl number, $Br = \Pr Ec$ is the Brinkmann number, $Ec = \frac{u_s^2}{(C_p)_f (T_s - T_\infty)}$ refers Eckert number, $\lambda_v = d\sqrt{\frac{u_s}{2l\nu_f}}$ is the velocity slip parameter, $\lambda_T = \frac{h_s}{\kappa_f}\sqrt{\frac{2l\nu_f}{u_s}}$ is the thermal slip parameter.

The parameters of technical concern within this investigation are skin friction coefficient and Nusselt number, stated as[4]

$$C_f = \frac{2\mu_{nf}(T)\left.\frac{\partial u}{\partial y}\right|_{y=0}}{\rho_f u_s^2}, \mathrm{Nu_x} = -\frac{\kappa_{nf}}{\kappa_f}\frac{\left.x\frac{\partial T}{\partial y}\right|_{y=0}}{(T_s - T_\infty)} \quad \ldots(14)$$

Imposing the transformations in Eq. (10), above expressions are acquired as

$$C_f\sqrt{\mathrm{Re}} = \frac{\mu_{nf}}{\mu_f}\frac{\sqrt{2}}{\left(1-\frac{\theta}{\theta_s}\right)} f''(0), \frac{\mathrm{Nu_x}}{\sqrt{\mathrm{Re}}} = -\frac{\kappa_{nf}}{\kappa_f}\frac{1}{\sqrt{2}}\theta'(0) \quad \ldots(15)$$

where $\mathrm{Re} = \frac{u_s l}{\nu_f}$ is the Reynolds number.

**Mathematical procedure**

The nonlinear differential equation framework (11)-(12) along boundary conditions (13) is functioned with spectral relaxation approach. The elementary step in this method is to formulate the differentiation matrix **D** to estimate the differential coefficients of unknown variables, that is

$$\frac{df}{d\eta} = \sum_{i=0}^{K}\mathbf{D}_{ji} f(\zeta_i) = \mathbf{Df}, \qquad \mathrm{j} = 0,1,...,\mathrm{K} \quad \ldots(16)$$

in which $\mathbf{f} = \left[f(\zeta_0), f(\zeta_1),..., f(\zeta_k)\right]^T$ is the vector function at $K+1$ grid points, and $\mathbf{D} = 2D/\eta_\infty$, where $\eta_\infty$ is a delimited length opted to tackle the infinite boundary conditions, and $\zeta$ is the transformation variable for distance $[0, \eta_\infty]$ to $[-1,1]$. Now, employing the transformation $f' = h$ to reduce the order of the differential equation. Therefore, after modifying the equations and practicing the iteration scheme (11)-(13) is derived as

$$\frac{h''_{r+1}}{\left(1-\frac{\theta_r}{\theta_s}\right)} + \frac{h'_{r+1}\theta'_r}{\theta_s\left(1-\frac{\theta_r}{\theta_s}\right)^2} + \frac{\nu_f}{\nu_{nf}} f_r h'_{r+1} = 2\frac{\nu_f}{\nu_{nf}} h_r^2 - \frac{\mu_f}{\mu_{nf}} Qe^{-\alpha\eta} \quad \ldots(17)$$

$$f'_{r+1} = h_{r+1} \quad \ldots(18)$$

$$\frac{\kappa_{nf}}{\kappa_f}\theta''_{r+1} + \Pr\frac{(\rho C_p)_{nf}}{(\rho C_p)_f}(f_{r+1}\theta'_{r+1} - h_{r+1}\theta_{r+1}) = -\frac{\mu_{nf}}{\mu_f}\frac{Br}{\left(1-\frac{\theta_{r+1}}{\theta_s}\right)} h'^2_{r+1} \quad \ldots(19)$$

with boundary conditions

$$f_{r+1}(0) = 0, \mathrm{h_{r+1}}(0) = 1 + \lambda_v h'_{r+1}(0), \theta'_{\mathrm{r+1}}(0) = -\lambda_T\left[1 - \theta_{r+1}(0)\right]$$
$$h_{r+1}(\infty) \to 0, \theta_{\mathrm{r+1}}(\infty) \to 0 \quad \ldots(20)$$

Now implementing the Chebyshev pseudo-spectral method in equations (17)-(20)

$$A_1\mathbf{h}_{r+1} = B_1, \mathrm{h_{r+1}}(\zeta_K) - \lambda_v h'_{r+1}(\zeta_K) = 1, \mathrm{h_{r+1}}(\zeta_0) = 0 \quad \ldots(21)$$

$$A_2\mathbf{f}_{r+1} = B_2,\ f_{r+1}(\zeta_K) = 0 \quad \ldots(22)$$

$$A_3\boldsymbol{\theta}_{r+1} = B_3, \theta'_{\mathrm{r+1}}(\zeta_K) = -\lambda_T\left[1 - \theta_{r+1}(\zeta_K)\right], \theta_{\mathrm{r+1}}(\zeta_0) = 0 \quad \ldots(23)$$

where

$$\mathrm{A_1} = \mathrm{diag}\left[\left(1-\frac{\boldsymbol{\theta}_\mathrm{r}}{\theta_\mathrm{s}}\right)^{-1}\right]\mathbf{D}^2 + \mathrm{diag}\left[\boldsymbol{\theta}'_\mathrm{r}\left(1-\frac{\boldsymbol{\theta}_\mathrm{r}}{\theta_\mathrm{s}}\right)^{-2}\right]$$
$$\frac{1}{\theta_\mathrm{s}}\mathbf{D} + \frac{\nu_\mathrm{f}}{\nu_\mathrm{nf}}\mathrm{diag}\left[\mathbf{f}_\mathrm{r}\right]\mathbf{D}, \mathrm{B_1} = 2\frac{\nu_\mathrm{f}}{\nu_\mathrm{nf}}\mathbf{h}_\mathrm{r}^2 - \frac{\mu_\mathrm{f}}{\mu_\mathrm{nf}}\mathrm{Qe}^{-\alpha\eta}$$

$$A_2 = \mathbf{D},\ B_2 = \mathbf{h}_{r+1}$$

$$A_3 = \frac{\kappa_{nf}}{\kappa_f}\mathbf{D}^2 + \mathrm{Pr}\frac{(\rho C_p)_{nf}}{(\rho C_p)_f}(\mathrm{diag}[\mathbf{f}_{r+1}]$$

$$\mathbf{D} - \mathrm{diag}[\mathbf{h}_{r+1}]\mathbf{I}),\ B_3 = -\mathrm{Br}\frac{\mu_{nf}}{\mu_f}\left(1-\frac{\boldsymbol{\theta}_{r+1}}{\theta_s}\right)^{-1}\mathbf{h}'^2_{r+1}$$

subscript $r$ represents the iteration number, diag [ ] stands for diagonal matrix of order $(K+1)\times(K+1)$, $\mathbf{I}$ is the identity matrix, $\mathbf{f}$ , $\mathbf{h}$, and $\boldsymbol{\theta}$ are evaluation of functions $f$ , $h$, and $\theta$ at the grid points, respectively. The iteration process is initiated with the following initial guesses

$$f_0(\eta) = 0,\ \mathrm{h}_0(\eta) = \frac{1}{2}e^{-\eta/\lambda_v},\ \theta_0(\eta) = \frac{1}{2}e^{-\eta\lambda_T} \qquad \ldots(24)$$

and repeated until the below convergence condition is accomplished

$$\left\{\left\|f_{r+1} - f_r\right\|, \left\|h_{r+1} - h_r\right\|, \left\|\theta_{r+1} - \theta_r\right\|\right\} < \varepsilon_r \qquad \ldots(25)$$

where $\varepsilon_r$ refers to error tolerance.

## Results and Discussion

The present section depicts the impact of pertinent parameters, nanoparticle volume fraction $(\varphi)$, modified Hartman number $(Q)$, dimensionless parameter $(\alpha)$, velocity slip parameter $(\lambda_v)$, Brinkmann number $(Br)$, and thermal slip parameter $(\lambda_T)$ on momentum and temperature distribution profiles through figures 3-14. The constant values of these parameters are considered as $\theta_s = 2, \varphi = 0.1, \mathrm{Q} = 1, \alpha = 0.5, \lambda_v = 1, \mathrm{Pr} = 7, \mathrm{Br} = 1,$ and $\lambda_T = 0.5$. Variation of skin drag factor and Nusselt number are contemplated via numerical data in Table 2. It is deduced from the table that skin drag factor is a growing function of $Q, \lambda_v, \mathrm{Br},$ and $\lambda_T$, whereas it reduces with growth in $\varphi$ and $\alpha$. Further,

Table 2 — Numeric data of $f''(0)$ and $\theta'(0)$ at discrete estimation of physical variables for SWCNT-water and MWCNT-water nanofluids when $\theta_s = 2$ and $\mathrm{Pr} = 7$

| $\varphi$ | $Q$ | $\alpha$ | $\lambda_v$ | $Br$ | $\lambda_T$ | $-f''(0)$ | | $-\theta'(0)$ | |
|---|---|---|---|---|---|---|---|---|---|
| | | | | | | SWCNT-water | MWCNT-water | SWCNT-water | MWCNT-water |
| 0.05 | 1 | 0.5 | 1 | 1 | 0.5 | 0.26410544 | 0.25525120 | 0.39289538 | 0.395624814 |
| 0.10 | | | | | | 0.27251640 | 0.25638064 | 0.37039371 | 0.375305206 |
| 0.15 | | | | | | 0.27869045 | 0.25660935 | 0.34993484 | 0.356824690 |
| 0.20 | | | | | | 0.28270666 | 0.25582606 | 0.33058545 | 0.339344944 |
| 0.25 | | | | | | 0.28460868 | 0.25392513 | 0.31185577 | 0.322411097 |
| 0.10 | 2 | | | | | 0.13595225 | 0.11396772 | 0.38250262 | 0.387088802 |
| | 3 | | | | | 0.01700983 | -0.01001595 | 0.38982150 | 0.394148514 |
| | 4 | | | | | -0.09040358 | -0.12195654 | 0.39483044 | 0.398932902 |
| | 5 | | | | | -0.18940247 | -0.22511352 | 0.39849080 | 0.402391580 |
| | 1 | 1.0 | | | | 0.31265738 | 0.29872895 | 0.36227937 | 0.367402507 |
| | | 1.5 | | | | 0.33799537 | 0.32531860 | 0.35699186 | 0.362272633 |
| | | 2.0 | | | | 0.35514217 | 0.34326155 | 0.35352105 | 0.358902282 |
| | | 2.5 | | | | 0.36750192 | 0.35616961 | 0.35114103 | 0.356585323 |
| | | 0.5 | 2 | | | 0.17056287 | 0.16116077 | 0.36871005 | 0.373730078 |
| | | | 3 | | | 0.12439896 | 0.11776138 | 0.36761985 | 0.372719216 |
| | | | 4 | | | 0.09796889 | 0.09283805 | 0.36689201 | 0.372045852 |
| | | | 5 | | | 0.08082468 | 0.07664245 | 0.36637674 | 0.371569602 |
| | | | 1 | 2 | | 0.27660015 | 0.26096423 | 0.36287682 | 0.367949691 |
| | | | | 3 | | 0.27637062 | 0.26077568 | 0.35686492 | 0.362136600 |
| | | | | 4 | | 0.27613578 | 0.26058279 | 0.35078964 | 0.356265116 |
| | | | | 5 | | 0.27589541 | 0.26038539 | 0.34464902 | 0.350333505 |
| | | | | 1 | 1.0 | 0.27063057 | 0.25527608 | 0.59063065 | 0.602889379 |
| | | | | | 1.5 | 0.26600879 | 0.25084967 | 0.73941932 | 0.758471330 |
| | | | | | 2.0 | 0.26242419 | 0.24739085 | 0.84642873 | 0.871272015 |
| | | | | | 2.5 | 0.25956088 | 0.24461203 | 0.92721403 | 0.956928052 |

Table 3 — Evaluation of the data concerning $-\theta'(0)$ for various Prandtl number values at $\theta_s \to \infty$, $\varphi = 0 = Q = \lambda_v = Br, \lambda_T \to \infty$ with $f''(0) = -1.28180983$

| *Pr* | Magyari and Keller[20] | Mukhopadhyay and Gorla[21] | Present results |
|---|---|---|---|
| 1 | 0.954782 | 0.9547 | 0.954787245 |
| 2 | | 1.4714 | 1.471459374 |
| 3 | 1.869075 | 1.8691 | 1.869072771 |
| 5 | 2.500135 | 2.5001 | 2.500130986 |
| 10 | 3.660379 | 3.6603 | 3.660371721 |

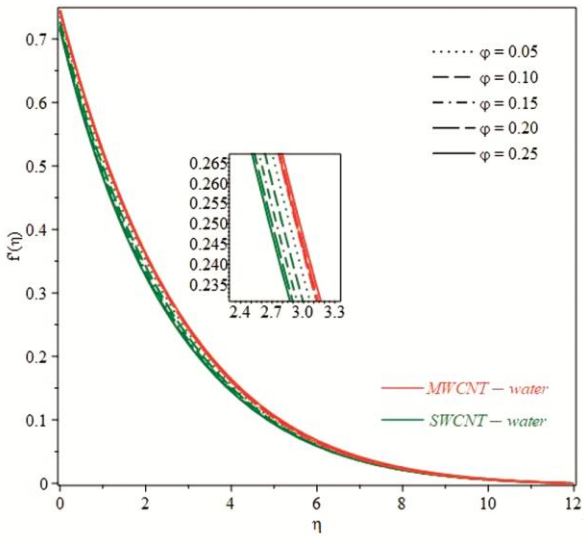


Fig. 3 — Dynamical influence of $\varphi$ over $f'(\eta)$

the Nusselt number enhances for $\varphi$, $\alpha, \lambda_v$ and $Br$ and diminishes for $Q$ and $\lambda_T$. Further, the methodology adopted in this study is validated, and its accuracy is evaluated by comparing the present results with those presented inprior literature[20,21]. The current results closely correspond to previous data, presented in Table 3, thus confirming their relevance and accuracy.

The impact of CNT particles concentration $(\varphi)$ on fluid flow and thermal profile are depicted in the Figs 3 and 4. The momentum profile diminishes in the case of SWCNT particles, and there appears to be a nominal growth in the case of MWCNT particles for enlargement in the solid volume fraction parameter. On the contrary, both nanoparticles have an enormous expansion in temperature profile and boundary layer thickness. From a physical perspective, the inclusion of solid particles causes fluid friction irreversibility, hence the momentum deficiency in the flow; also, due

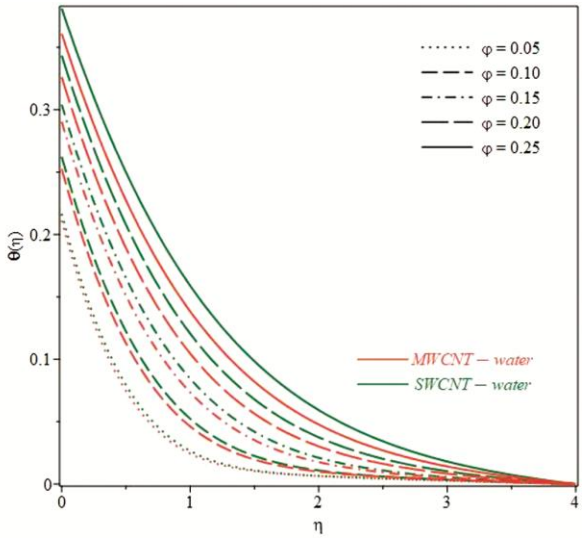


Fig. 4 — Thermal influence of $\varphi$ over $\theta(\eta)$

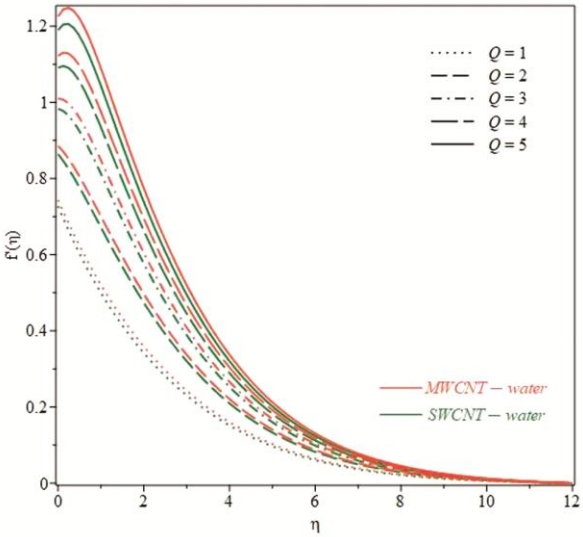


Fig. 5 — Dynamical influence of $Q$ over $f'(\eta)$

to increased resistance in fluid particles, more thermal energy is produced, which drives a rise in temperature distribution.

Variations in momentum and heat profiles against improved Hartman number $(Q)$ are illustrated in Figs 5 and 6, respectively. It is determined that the fluid flow and width of the momentum boundary layer increase, whereas the temperature profile exhibits a cross-flow behavior with higher values of $(Q)$. Moreover, MWCNT-water nanofluid attains a higher velocity profile as compared to SWCNT-water. Physically, the induced wall parallel Lorentz force

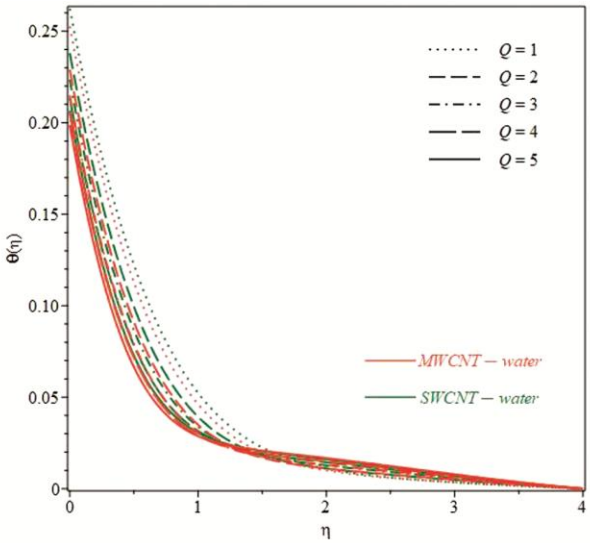


Fig. 6 — Thermal influence of Q over $\theta(\eta)$

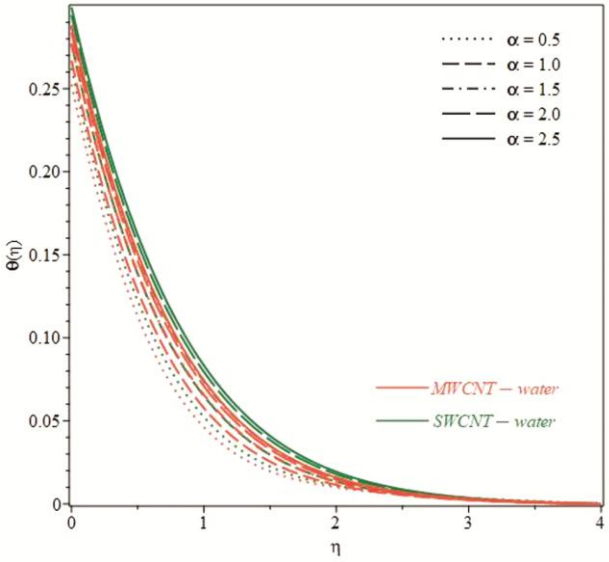


Fig. 8 — Thermal influence of $\alpha$ over $\theta(\eta)$

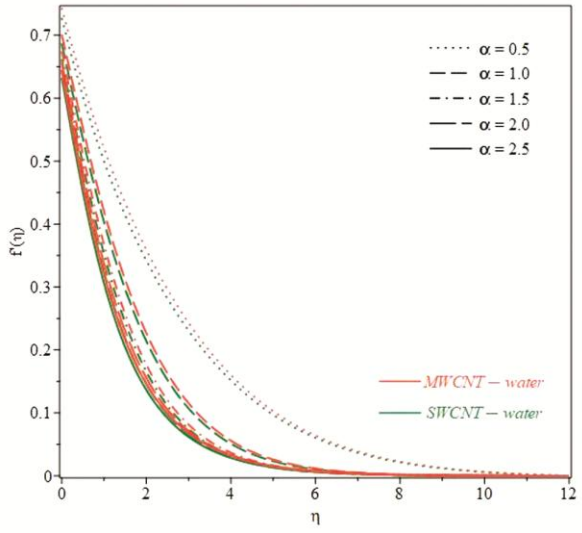


Fig. 7 — Dynamical influence of $\alpha$ over $f'(\eta)$

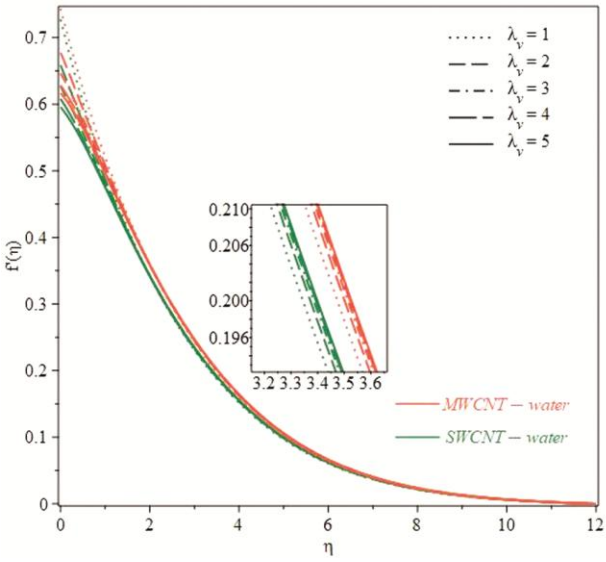


Fig. 9 — Dynamical influence of $\lambda_v$ over $f'(\eta)$

drives the fluid flow in the $x-$ direction, increases the fluid velocity, and reduces the temperature profile near the plate surface.

The dimensionless parameter $(\alpha)$ impact on fluid velocity and temperature are shown in Figs 7 and 8, respectively. At higher values of $\alpha$, there is a notable decrease in fluid velocity alongside a significant enhancement in the heat distribution profile. This is an outcome of contraction within the momentum boundary layer extent. Furthermore, SWCNT-water nanofluid attains lower velocity and higher temperature profile.

Figs 9 and 10 illustrate the influence of velocity slip parameter $(\lambda_v)$ on momentum and thermal distribution profiles. The fluid velocity and temperature profiles do not show significant variation against the increasing effect of the velocity slip parameter. There appears to be a deceleration in fluid velocity near the plate surface and a minor improvement in fluid temperature. Physically, due to the slip effect, the flow velocity contiguous to the Riga plate gets lagged compared to the stretching velocity, which causes flow retardation.

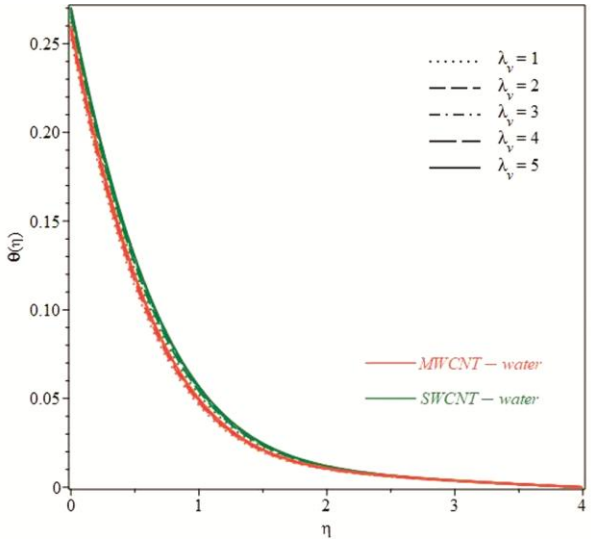


Fig. 10 — Thermal influence of $\lambda_v$ over $\theta(\eta)$

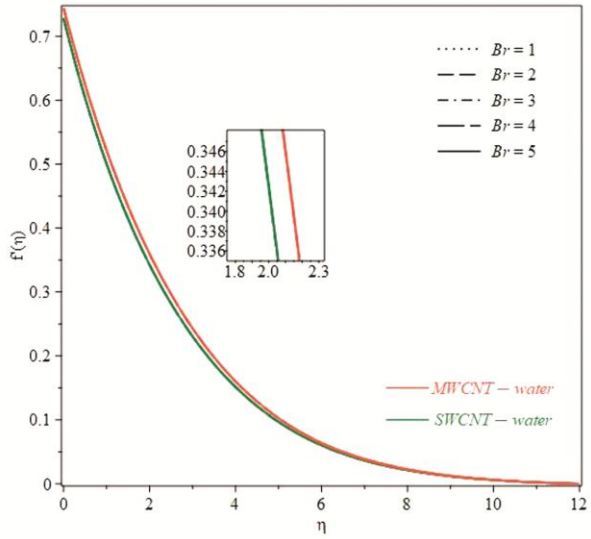


Fig. 11 — Dynamical influence of $Br$ over $f'(\eta)$

The effect of Brinkmann number $(Br)$ on the velocity and thermal profiles is displayed in the Figs 11 and 12, respectively. The velocity profile shows no variation against Brinkmann number. The thermal profile and the width of its boundary layer get enlarged with an increment in $Br$ values. Physically, increasing Brinkmann number values indicates more significant heat generation due to viscous dissipation, which boosts the fluid temperature for both kinds of nanofluids.

Figs 13 and 14 manifest the consequences of thermal slip parameter $(\lambda_T)$ on velocity and heat profiles. The fluid velocity experiences a marginal rise as the

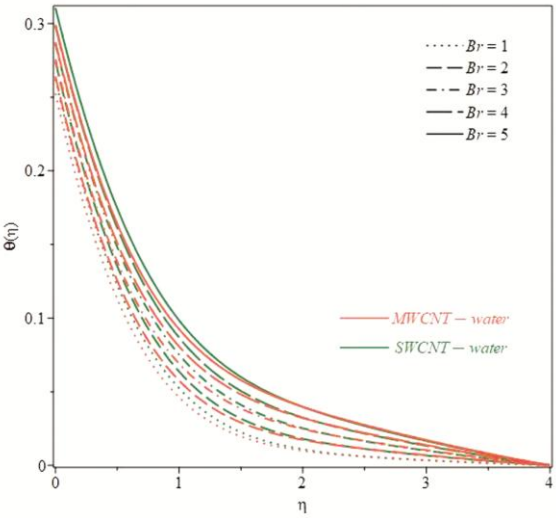


Fig. 12 — Thermal influence of $Br$ over $\theta(\eta)$

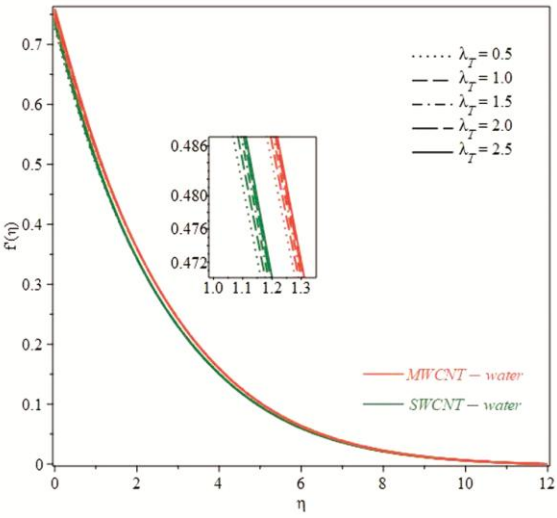


Fig. 13 — Dynamical influence of $\lambda_T$ over $f'(\eta)$

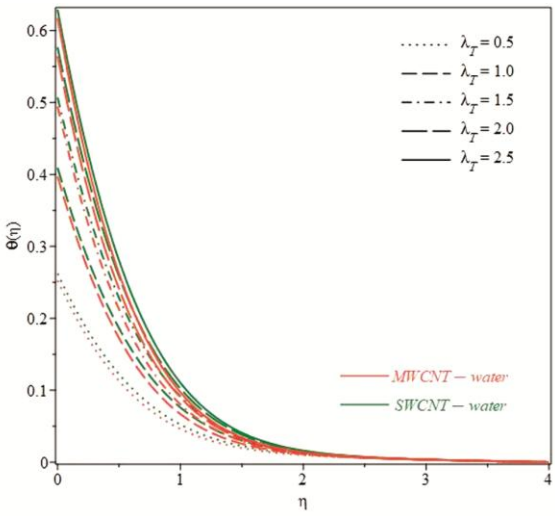


Fig. 14 — Thermal influence of $\lambda_T$ over $\theta(\eta)$

values of $\lambda_T$ increase. Temperature and thermal boundary layer are perceived to be increased under higher thermal slip effects. Additionally, the temperature is observed to be higher in the case of the SWCNT-water nanofluid.

## Conclusion

A computational analysis was performed to study the behavior of CNT-water nanofluid flowing over an exponentially stretched Riga plate. This analysis included the examination of viscous dissipation, temperature-dependent dynamic viscosity, and velocity and thermal slip effects. The mathematical model has been solved using the spectral relaxation method. The fluid velocity profile possesses a contrary response for SWCNT and MWCNT nanoparticle volume fraction parameters, whereas temperature and surface heat flux boost up for the rise in solid volume fraction. For both nanofluids, skin drag factor and Nusselt number retain a similar trend against velocity slip parameter and Brinkman number and contrary behavior for all other parameters. The velocity profile increases and thermal profile decreases with enhancement in modified Hartman number, whereas both profiles evince reversal movement for dimensionless parameter $\alpha$. Augmentation in velocity slip impact upgrades both the velocity and temperature profiles. Temperature is an increasing function of Brinkman number and thermal slip parameter.

## Acknowledgement

One of the authors, Kiran Kunwar Chouhan, expresses gratitude to the University Grant Commission (UGC), New Delhi, for the financial assistance provided under UGC Reference Number 1202 and Grant Number F. No. 16-6 (DEC.2018)/ 2019(NET/CSIR) on April 2, 2019.

## References

1 Choi S U S & Eastman J A, Enhancing thermal conductivity of fluids with nanoparticles, *Mater Sci*, 231 (1995) 99.
2 Kamali R & Binesh A R, Numerical investigation of heat transfer enhancement using carbon nanotube-based non-Newtonian nanofluids, *Int Commun Heat Mass Transf*, 37 (2010) 1153.
3 Prabhavathi B, Reddy P S & Vijaya R B, Heat and mass transfer enhancement of SWCNTs and MWCNTs based Maxwell nanofluid flow over a vertical cone with slip effects, *Powder Technol*, 30 (2018) 253.
4 Chaudhary S & Chouhan K K, Ohmic-viscous dissipation in MHD slip flow of Cu-blood nanofluid over a stretching surface along nanoparticle shapes, *Indian J Pure Appl Phys*, 59 (2021) 559.
5 Eswaramoorthi S, Loganathan K, Jain R & Gyeltshen S, Thermal radiation and viscous dissipation impacts of water and kerosene-based carbon nanotubes over a heated riga sheet, *J Nanomater*, 2022 (2022) 1.
6 Gailitis A K & Lielausis O A, On the possibility of drag reduction of a flat plate in an electrolyte, *Appl Magnetohydrodyn Trudy Inst Fisiky AN Latvia SSR*, 12 (1961) 143.
7 Ayub M, Abbas T & Bhatti M M, Inspiration of slip effects on electromagnetohydrodynamics (EMHD) nanofluid flow through a horizontal Riga plate, *Eur Phys J Plus*, 131 (2016) 1.
8 Nasir N A, Ishak A & Pop I, Stagnation point flow and heat transfer past a permeable stretching/shrinking Riga plate with velocity slip and radiation effects, *J Zhejiang Univ Sci A*, 20 (2019) 290.
9 Shamshuddin M D, Mabood F, Rajput G R, Be´g O A & Badruddin I A, Thermo-solutal dual stratified convective magnetized fluid flow from an exponentially stretching Riga plate sensor surface with thermophoresis, *Int Commun Heat Mass Transf*, 134 (2022) 105997.
10 Brinkman H C, Heat effects in capillary flow I, *Appl Sci Res*, 2 (1951) 120.
11 Ghalambaz M, Sabour M & Pop I, Free convection in a square cavity filled by a porous medium saturated by a nanofluid: Viscous dissipation and radiation effects, *Eng Sci Technol Int J*, 19 (2016) 1244.
12 Chaudhary S & Kanika K M, Viscous dissipation and Joule heating in MHD Marangoni boundary layer flow and radiation heat transfer of Cu–water nanofluid along particle shapes over an exponential temperature, *Int J Comput Math*, 97 (2020) 943.
13 Mahesh R, Mahabaleshwar U S, Kumar P V, O¨ ztop H F & Abu-Hamdeh N, Impact of radiation on the MHD couple stress hybrid nanofluid flow over a porous sheet with viscous dissipation, *Results Eng*, 17 (2023) 100905.
14 Sinha A, Shit G C & Ranjit N K, Peristaltic transport of MHD flow and heat transfer in an asymmetric channel: Effects of variable viscosity, velocity-slip and temperature jump, *Alex Eng J*, 54 (2015) 691.
15 Chaudhary S & Choudhary M K, Partial slip and thermal radiation effects on hydromagnetic flow over an exponentially stretching surface with suction or blowing, *Therm Sci*, 22 (2018) 797.
16 Gbadeyan J A & Titiloye E O & Adeosun A T, Effect of variable thermal conductivity and viscosity on Casson nanofluid flow with convective heating and velocity slip, *Heliyon*, 6 (2020) e03076.
17 Krishna M V, Hall and ion slip effects on radiative MHD rotating flow of Jeffreys fluid past an infinite vertical flat porous surface with ramped wall velocity and temperature, *Int Commun Heat Mass Transf*, 126 (2021) 105399.
18 Abbas N, Nadeem S & Issakhov A, Transportation of modified nanofluid flow with time dependent viscosity over a Riga plate: Exponentially stretching, *Ain Shams Eng J*, 12 (2021) 3967.
19 Nadeem S, Abbas N & Malik M Y, Heat transport in CNTs based nanomaterial flow of non-Newtonian fluid having electro magnetize plate, *Alex Eng J*, 59 (2020) 3431.
20 Magyari E & Keller B, Heat and mass transfer in the boundary layers on an exponentially stretching continuous surface, *J Phys D Appl Phys*, 32 (1999) 577.
21 Mukhopadhyay S & Gorla R S, Effects of partial slip on boundary layer flow past a permeable exponential stretching sheet in presence of thermal radiation, *Heat Mass Transf*, 48 (2012) 1773.